2-1-2023

Artificial intelligence-based multi-class histopathologic classification of kidney neoplasms

Dibson D. Gondim

Khaleel I. Al-Obaidy

Muhammad T. Idrees

John N. Eble

Liang Cheng

Journal of Pathology Informatics 14 (2023) 100299

Contents lists available at ScienceDirect

Journal of Pathology Informatics

journal homepage: www.elsevier.com/locate/jpi

Artificial intelligence-based multi-class histopathologic classification of kidney neoplasms

Dibson D. Gondim [a,*], Khaleel I. Al-Obaidy [b], Muhammad T. Idrees [c], John N. Eble [c], Liang Cheng [d]

[a] Department of Pathology, University of Louisville School of Medicine, Louisville, KY 40202, USA
[b] Department of Pathology and Laboratory Medicine, Henry Ford Health, 2799 West Grand Blvd, Detroit, MI 48202, USA
[c] Department of Pathology and Laboratory Medicine, Indiana University School of Medicine, Indianapolis, IN 46202, USA
[d] Department of Pathology and Laboratory Medicine, Brown University Warren Alpert Medical School, Lifespan Academic Medical Center, and the Legorreta Cancer Center at Brown University, Providence, RI, USA

ARTICLE INFO

Keywords::
Renal cell carcinoma
Renal oncocytoma
Metanephric adenoma
Histopathology
Artificial intelligence
Digital pathology

ABSTRACT

Artificial intelligence (AI)-based techniques are increasingly being explored as an emerging ancillary technique for improving accuracy and reproducibility of histopathological diagnosis. Renal cell carcinoma (RCC) is a malignancy responsible for 2% of cancer deaths worldwide. Given that RCC is a heterogenous disease, accurate histopathological classification is essential to separate aggressive subtypes from indolent ones and benign mimickers. There are early promising results using AI for RCC classification to distinguish between 2 and 3 subtypes of RCC. However, it is not clear how an AI-based model designed for multiple subtypes of RCCs, and benign mimickers would perform which is a scenario closer to the real practice of pathology. A computational model was created using 252 whole slide images (WSI) (clear cell RCC: 56, papillary RCC: 81, chromophobe RCC: 51, clear cell papillary RCC: 39, and, metanephric adenoma: 6). 298,071 patches were used to develop the AI-based image classifier. 298,071 patches (350 × 350-pixel) were used to develop the AI-based image classifier. The model was applied to a secondary dataset and demonstrated that 47/55 (85%) WSIs were correctly classified. This computational model showed excellent results except to distinguish clear cell RCC from clear cell papillary RCC. Further validation using multi-institutional large datasets and prospective studies are needed to determine the potential to translation to clinical practice.

Introduction

Renal cell carcinoma (RCC) is the seventh most common type of malignancy worldwide, accounting for approximately 2% of cancer diagnoses and deaths.[1] The diagnosis of RCC is multifaceted. In the developing world, most cases of RCC are detected incidentally in radiology studies. Symptomatic cases present one or more symptoms (e.g., hematuria, flank/back pain, palpable mass, weight loss, and leukocytosis) which prompts radiology studies and detection of a renal mass.[2] However, not all renal parenchymal masses in radiology studies represent RCC. Confirmation requires evaluation of a tissue sample by histopathology which is the gold-standard diagnostic technique. Histopathology allows distinction between RCC and benign renal neoplasms and enables subclassification and grading of RCC, essential for stratifying prognosis and making treatment decisions. Among the 4 most prevalent subtypes of RCC, clear cell renal cell carcinoma (ccRCC) is the most common and has the worst prognosis compared to papillary renal cell carcinoma (pRCC), chromophobe renal cell carcinoma (chRCC), and clear cell papillary renal cell carcinoma (ccpRCC).[3] Histopathological classification weighs heavily on recognition of morphologic patterns seen in the hematoxylin and eosin (H&E)-stained tissue section. In many cases, a confident diagnosis can be rendered based on the identification of specific morphologic patterns by a pathologist without the need for additional studies or referring the case for expert consultation. However, some places in the world experience a shortage of pathologists, a limited number of experts in genitourinary pathology for consultations and limited or no availability of ancillary studies such as immunohistochemistry.[4,5] With the advent of digital pathology, glass slides can be digitized into whole slide images (WSI) which are amenable to image analysis techniques.[6] AI-based image analysis techniques, more specifically convolutional neural networks, can recognize complex patterns and match them to specific categories enabling automated image classification in multiple health care and non-health care domains.[7–11] There are multiple publications exploring the use of AI for the diagnosis of RCC with promising results. However, the experimentation design is limited to

* Corresponding author at: Department of Pathology, University of Louisville School of Medicine, Louisville, KY 40292, USA.
E-mail address: dibson.gondim@louisville.edu (D.D. Gondim).

http://dx.doi.org/10.1016/j.jpi.2023.100299
Received 1 June 2022; Received in revised form 3 February 2023; Accepted 11 February 2023
Available online 16 February 2023

classification between 2 and 3 different subtypes of RCC.[12–15] We aim to create a computation model that can distinguish between multiple subtypes of RCC (ccRCC, pRCC, chRCC, and ccpRCC) and benign renal neoplasms (oncocytoma and metanephric adenoma) which is a scenario that would have greater utility for potential translation into clinical practice. We evaluated the performance of the computational model on a WSI validation dataset and created a platform to allow the pathologist to correlate the AI results on WSIs.

Materials and methods

Dataset creation including annotation and patch extraction preprocessing pipeline

The project was approved by Institutional Review Boards (IRB). Nephrectomy specimens with the following diagnosis were selected: clear cell renal cell carcinoma (ccRCC), papillary renal cell carcinoma (pRCC), chromophobe renal cell carcinoma (chRCC), clear cell papillary renal cell carcinoma (ccpRCC), oncocytoma, and metanephric adenoma. The original diagnoses were rendered by pathologists with expertise in genitourinary pathology. All pathology reports and histology slides were reviewed by a pathologist with expertise in genitourinary pathology (DG) who selected representative H&E slides. Cases with more than one type of renal neoplasm were excluded. Slides were digitized into WSI using Philips IntelliSite Pathology Solution (Philips, the Netherlands) and corresponding 100x magnification TIFF files were downloaded and converted to JPEG. Protected health information was removed to anonymize the files. All areas containing tumor in each image were annotated by a pathologist (DG). Annotation consisted of creating a binary image overlay using Photoshop (Adobe, San Jose, CA). A python script was created to extract 350 × 350-pixel image patches from the areas of annotation. (Fig. 1).

Two separate datasets with no overlapping cases were created. The first dataset was used for AI-based patch classifier creation and the second dataset was used to validate WSI tumor classification.

AI-based patch classifier development

The patch classifier was created using Google AutoML Vision which is a commercial application programming interface (API) for the development of AI-based image classifiers.[16,17] This API is commercialized as a generic solution to create custom classifiers for automated image categorization. Given that generic images are different from pathology WSI in many aspects (e.g., WSIs commonly have gigabits in size), the preprocessing step using a python script to extract patches from the WSIs is fundamental to make images compatible with the API. The API receives as input the AI-model creation patch datasets and creates an image classifier as output. The classifier becomes hosted in a server and can be accessed via an API call on the internet using access credentials (Fig. 2).

Model performance evaluation

The computational model performance is evaluated at the patch- and WSI levels. The patch classifier performance is evaluated by the average precision of the area under the precision-recall curve (AuPRC) which determines accuracy of the classification of an individual patch. An example of patch classification is demonstrated in Fig. 2. Tumor classification on WSI consists of the percentage of concordance between the final computational model diagnosis based on the majority vote of aggregated classification of all patches and the ground-truth histopathological diagnosis rendered by a pathologist.

Visualization of results of WSI

A serverless web application was created to enable visualization of AI results on the WSI validation dataset interactively and correlation with histologic findings on WSI. The 100x magnification TIFF images were converted into deep zoom image files (DZI). OpenSeaDragon library was used to render the DZI-based whole slides images on a browser.[18] A semi-transparent overlay was created using cascading style sheets to allow visualization of the AI-model results.[19] The visualization includes classification of each patch with the probability of the patch belonging to the predicated label based on AI-based patch classifier results. The overlay can be toggled off to allow correlation with underlying morphology.

Results

A total of 252 WSIs were used to create the AI-based patch classifier (197 WSIs) and WSI-level tumor classification dataset (55 WSIs). The number of WSIs per category is in Table 1.

AI-based patch classifier creation and performance

The AI-based patch classifier was created using Google AutoML API.[16] The total number of non-overlapping patches used for AI-based patch classifier development was 298,071. The number of patches per category is provided in Table 2. The patches were randomly split into training (75%), testing (5%), and validation (20%) datasets and fed as input to the API.

After 1 h of training, the patch classifier showed an average precision based on AuPRC of 76% (Fig. 3). The final patch classifier was trained for 8 h, and the final model's average precision based on AuPRC of 93% for

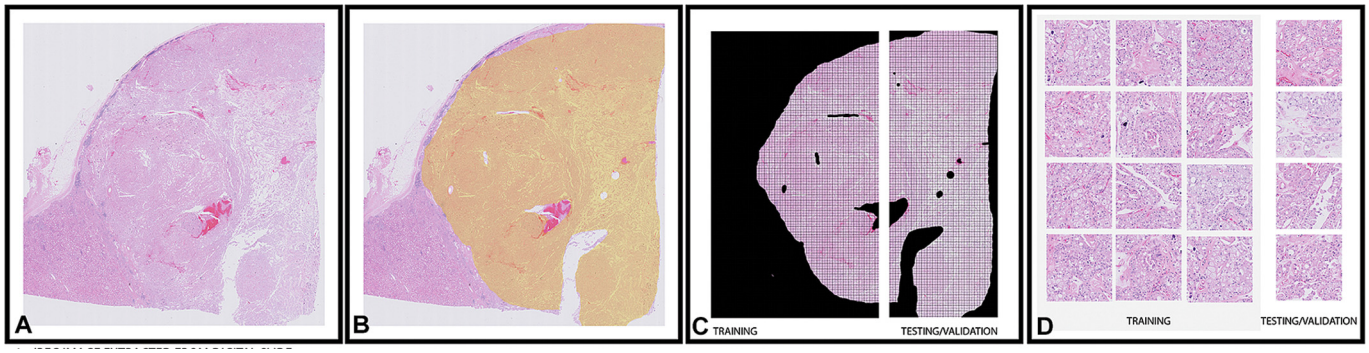

Fig. 1. Ground-truth annotation and extractions of patches. (A) JPEG image extracted from digital slide; (B) tumor selection (ground truth); (C) no overlap between patches used for training and testing/validation datasets; and (D) patches.

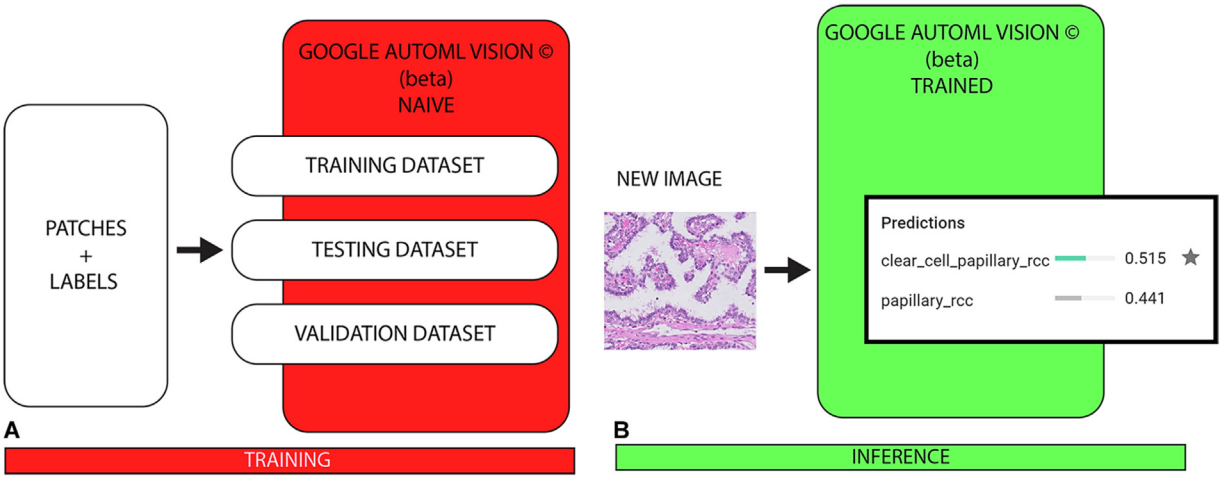

Fig. 2. Google AutoML Vision (beta) training and inference: (A) naïve and (B) trained.

Table 1
Number of WSIs per category used to create all the datasets.

Pathology	Cases
Clear cell renal cell carcinoma	56
Papillary renal cell carcinoma	81
Chromophobe renal cell carcinoma	51
Clear cell papillary renal cell carcinoma	19
Oncocytoma	39
Metanephric adenoma	6
Total	252

Table 2
Number of patches per category used to create the patch classifier on Google AutoML vision API.

Pathology	Patches
Clear cell renal cell carcinoma	53,018
Papillary renal cell carcinoma	53,712
Chromophobe renal cell carcinoma	52,750
Clear cell papillary renal cell carcinoma	37,834
Oncocytoma	52,230
Metanephric adenoma	48,527
Total	298,071

patch classification. At a 50% threshold, the precision was 88% and recall 86% (Fig. 3). The model showed the best performance to classify oncocytoma (94%) and worst performance for ccpRCC (47%). The confusion matrices of the 1- and 8-h models are in Fig. 3.

Whole slide image performance

The next step was to determine the model performance on the WSI validation dataset whose images were not used to create the patch classifier. The patch classifier was used to classify all patches with tumor in the WSI. The number of tumor patches per WSI ranged from 35 to 2,508 patched (average 985). The ratio of the number of most frequent patch diagnosis was divided by the total number of patches. This ratio ranged from 0.44 to 1. In 37/55 (67%) cases, the predominant patch accounted for more than 90% of all patches. The final tumor classification based on majority vote correctly classified 47/55 (85%) cases (ccRCC 11/13, pRCC 14/15, chRCC 10/11, ccpRCC 2/4, oncocytoma 8/9, and metanephric adenoma 2/3). All tumors that had a ratio above 0.77 were correctly classified. See Table 3 with detailed results, Table 4 for WSI-level confusion matrix and Fig. 4 shows a color-coded visual representation of the results.

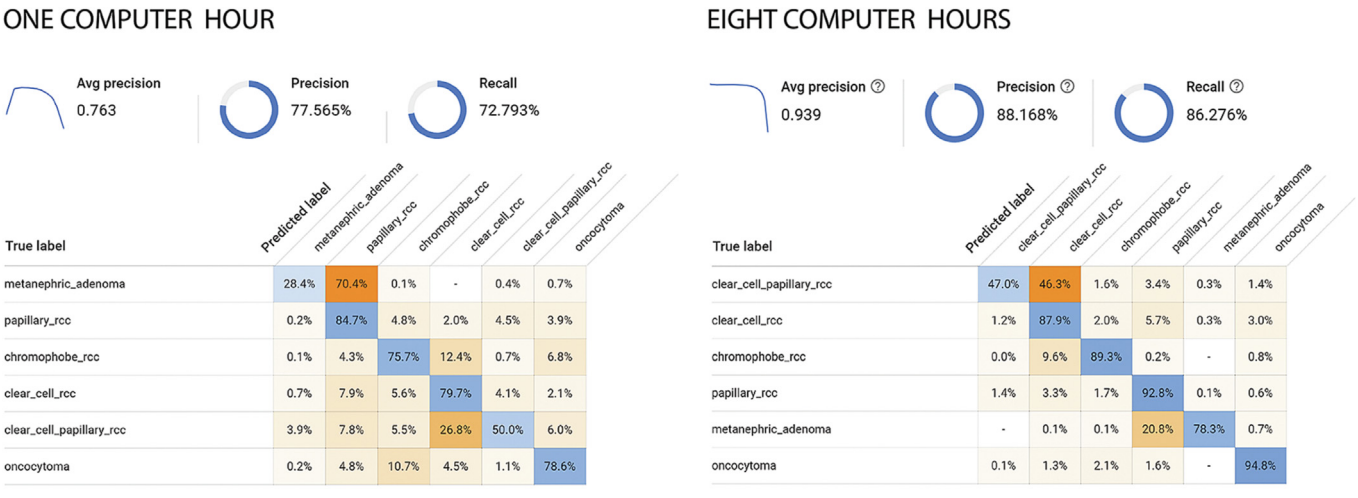

Fig. 3. Patch classification performance metrics AuPRC and confusions matrices for models after 1 and 8 h of training. The confusion matrices show how often the model classified each label correctly (in blue), and which labels were most often misclassified for that label (in orange).

Table 3
WSI-level validation. The most frequent patch label/all patches indicate the degree of heterogeneity of the patch classification. Ratios above 0.999 were approximated to 1.

Case	Diagnosis	AI Classification	Agreement	Most frequent/all patches ratio
1	clear cell RCC	clear cell RCC	TRUE	0.99
2	clear cell RCC	clear cell RCC	TRUE	0.99
3	clear cell RCC	clear cell RCC	TRUE	0.99
4	clear cell RCC	clear cell RCC	TRUE	0.98
5	clear cell RCC	clear cell RCC	TRUE	0.96
6	clear cell RCC	clear cell RCC	TRUE	0.96
7	clear cell RCC	clear cell RCC	TRUE	0.93
8	clear cell RCC	clear cell RCC	TRUE	0.92
9	clear cell RCC	clear cell RCC	TRUE	0.89
10	clear cell RCC	clear cell RCC	TRUE	0.85
11	clear cell RCC	clear cell RCC	TRUE	0.84
12	clear cell RCC	clear cell papillary RCC	FALSE	0.54
13	clear cell RCC	papillary RCC	FALSE	0.55
14	papillary RCC	papillary RCC	TRUE	1.00
15	papillary RCC	papillary RCC	TRUE	1.00
16	papillary RCC	papillary RCC	TRUE	1.00
17	papillary RCC	papillary RCC	TRUE	1.00
18	papillary RCC	papillary RCC	TRUE	1.00
19	papillary RCC	papillary RCC	TRUE	0.99
20	papillary RCC	papillary RCC	TRUE	0.99
21	papillary RCC	papillary RCC	TRUE	0.98
22	papillary RCC	papillary RCC	TRUE	0.97
23	papillary RCC	papillary RCC	TRUE	0.97
24	papillary RCC	papillary RCC	TRUE	0.97
25	papillary RCC	papillary RCC	TRUE	0.96
26	papillary RCC	papillary RCC	TRUE	0.95
27	papillary RCC	papillary RCC	TRUE	0.93
28	papillary RCC	clear cell RCC	FALSE	0.44
29	chromophobe RCC	chromophobe RCC	TRUE	1.00
30	chromophobe RCC	chromophobe RCC	TRUE	1.00
31	chromophobe RCC	chromophobe RCC	TRUE	0.99
32	chromophobe RCC	chromophobe RCC	TRUE	0.99
33	chromophobe RCC	chromophobe RCC	TRUE	0.99
34	chromophobe RCC	chromophobe RCC	TRUE	0.98
35	chromophobe RCC	chromophobe RCC	TRUE	0.94
36	chromophobe RCC	chromophobe RCC	TRUE	0.90
37	chromophobe RCC	chromophobe RCC	TRUE	0.85
38	chromophobe RCC	chromophobe RCC	TRUE	0.74
39	chromophobe RCC	clear cell RCC	FALSE	0.67
40	clear cell papillary RCC	clear cell papillary RCC	TRUE	0.99
41	clear cell papillary RCC	clear cell papillary RCC	TRUE	0.54
42	clear cell papillary RCC	clear cell RCC	FALSE	0.64
43	clear cell papillary RCC	clear cell RCC	FALSE	0.60
44	oncocytoma	oncocytoma	TRUE	1.00
45	oncocytoma	oncocytoma	TRUE	0.99
46	oncocytoma	oncocytoma	TRUE	0.99
47	oncocytoma	oncocytoma	TRUE	0.99
48	oncocytoma	oncocytoma	TRUE	0.98
49	oncocytoma	oncocytoma	TRUE	0.98
50	oncocytoma	oncocytoma	TRUE	0.84
51	oncocytoma	oncocytoma	TRUE	0.75
52	oncocytoma	papillary RCC	FALSE	0.46
53	metanephric adenoma	metanephric adenoma	TRUE	1.00
54	metanephric adenoma	metanephric adenoma	TRUE	0.97
55	metanephric adenoma	papillary RCC	FALSE	0.77

Table 4
WSI-level classification confusion matrix based on the majority vote of all classification of all tumor patches.

	AI Classification					
Pathology	**Clear cell RCC**	**Papillary RCC**	**Chromophobe RCC**	**Clear cell papillary RCC**	**Oncocytoma**	**Metanephric adenoma**
Clear cell RCC	11	1	1	2	0	0
Papillary RCC	1	14	0	0	0	0
Chromophobe RCC	1	0	10	0	0	0
Clear cell papillary RCC	2	0	0	2	0	0
Oncocytoma	0	1	0	0	8	0
Metanephric adenoma	0	1	0	0	0	2

Evaluation of random sample of patches by a pathologist

A random sample of tumor patches of the WSI dataset that were classified with more than 90% probability of belonging to the predicted label was examined by a pathologist (DG). Examination of the sample patches revealed typical diagnostic histopathological features (Fig. 5). Patches of ccRCC showed small nests of clear cells and alveolar structures of clear cells filled with blood (Fig. 5a). Patches of pRCC showed papillary projections longitudinally and tangentially cut either lined by cells with an amphophilic cytoplasm (pRCC type 1 pattern) or eosinophilic cytoplasm (pRCC type 2 pattern) (Fig. 5b). Patches of chRCC showed well-defined plant-like cell borders, perinuclear halos, and a mixture of cells with abundant pale cytoplasm and others with more scanty eosinophilic cytoplasm (Fig. 5c). Patches of ccpRCC showed stubby papillae and tubulocystic structures lined by clear cells (Fig. 5d). Patches of oncocytoma showed nests of eosinophilic cells embedded in fibrous or edematous stroma as well as small cysts filled with blood or proteinaceous material (Fig. 5e). Patches of metanephric adenoma showed compact tubular structures composed of cells with a high nuclear to cytoplasmic ratio (Fig. 5f).

Evaluation of whole slide images and AI output by a pathologist

The web application used for correlation of histopathological evaluation with AI results can be accessed through the provided interactive Supplementary material. Overall, the model classifies patches containing clear cells as either ccRCC or ccpRCC. Papillae were predominantly classified as pRCC or ccpRCC. However, no cases of ccpRCC were misclassified as ccRCC or vice versa. There was no significant overlap between oncocytoma and chRCC. A sole case of eosinophilic variant of chRCC was present in the dataset (Table 3, case 37). This case was correctly classified as chRCC (ratio, 0.85) on WSI. However, a subset of patches of this case where the nests of eosinophilic cells were separated by hypocellular stroma were misclassified as oncocytoma.

Discussion

AI-based models have been demonstrated to be viable technology for automated image classification tasks in health care and non-health care domains.[7–11] The application of AI to histopathology diagnosis is a field in rapid expansion and there has been a recent approval of commercial software for detection and grading of prostate cancer in the clinical setting by the FDA.[20]

To the best of our knowledge, this is the first study demonstrating a computational model that can distinguish between 6 subtypes of renal cell neoplasms with high accuracy, except the distinction between ccRCC from ccpRCC. The other caveat is related to classification of metanephric adenoma. Although there were only 3 metanephric adenomas in the WSI validation dataset and 2 of the 3 were correctly classified, the results still look promising because the 2 correctly classified cases had more than 1000 patches each and these patches were classified with a concordance ratio of 0.97 and close to 1.0, respectively. A misclassified metanephric adenoma had 77% of the patches classified as pRCC and approximately 20% classified as metanephric adenoma. Interestingly, the misclassified case had a predominant papillary architecture which was not present in the other 2 cases of metanephric adenoma.

Prior research on AI for RCC classification was limited to a distinction between 2 and 3 subtypes of RCC. Several investigators demonstrated AI-based models able to separate ccRCC, pRCC, and chRCC with accuracy above 90%.[12,13,21] Benchmarking of various convolutional neural networks is provided by Laleh et al.[21] Gayhart et al showed results approaching between 96% and 100% accuracy to separate ccRCC from chRCC using convolutional neural networks.[14] A pyramidal deep learning pipeline was demonstrated to distinguish between ccRCC and ccpRCC with high accuracy.[22,23] Such a pipeline has the potential to be complementary to this model where all the cases with a final label of ccRCC or ccpRCC could be fed into the other model that showed better accuracy separating tumors with clear cells. Cheng et al demonstrated a computational model with satisfactory performance distinguishing between ccRCC and TFE3 Xp11.2 translocation RCC, a rare type of RCC.[15]

We selected the 4 most common subtypes of RCC (ccRCC, pRCC, chRCC, and ccPRCC) because they encompass approximately 95% of RCCs. In addition, oncocytoma was included because it is a benign neoplasm that accounts for 3%–7% of renal epithelial neoplasms and is diagnosed when RCC can be excluded.[24] Finally, the addition of metanephric adenoma, a rare benign tumor, did not add much to the model coverage, but the addition of another class made the multilabel classification more challenging. The coverage and accuracy of this model are closer to a system with potential clinical utility.

The 2016 World Health Organization classification documents 14 subtypes of RCC and 4 emerging/provisional entities.[25] An ideal classifier to

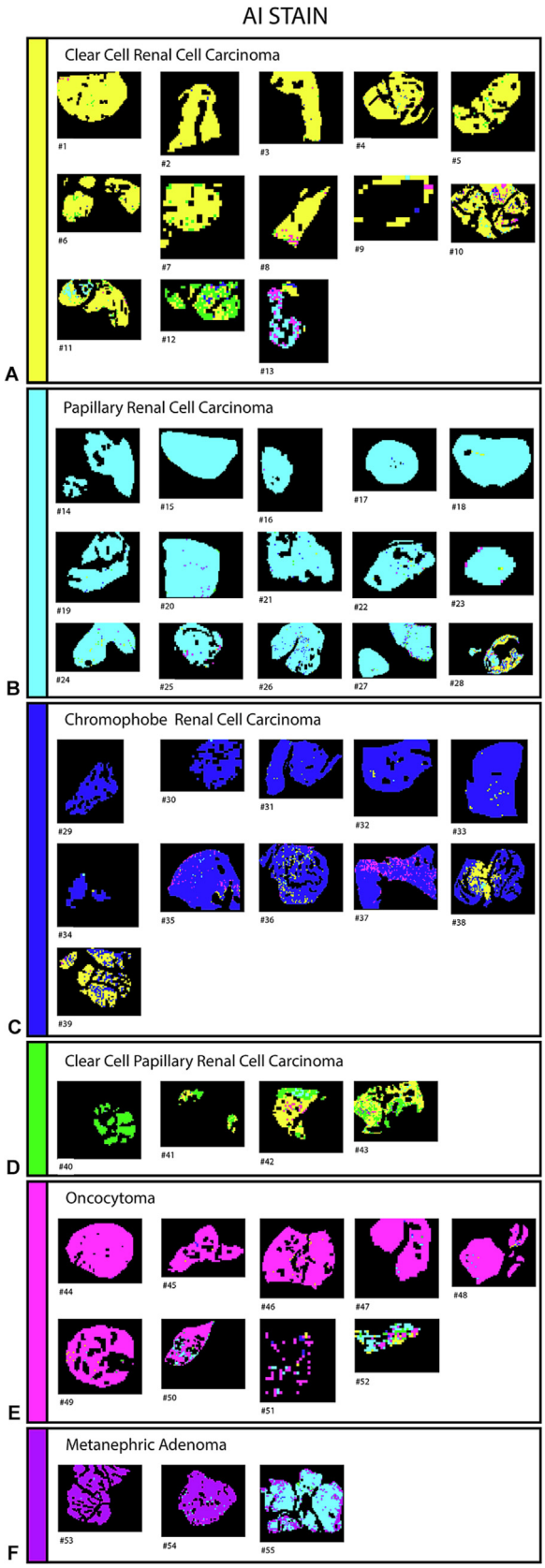

Fig. 4. Color-coded representation of the WSI-level results. (A) Yellow: clear cell renal cell carcinoma; (B) Cyan: papillary renal cell carcinoma; (C) Blue: chromophobe renal cell carcinoma; (D) Green: clear cell papillary renal cell carcinoma; (E) Pink: oncocytoma; and (F) Purple: metanephric adenoma.

be deployed in the clinical setting would be able to distinguish with high accuracy all subtypes of RCC, urothelial carcinoma, and non-RCC/non-urothelial carcinoma categories. The challenge to create such a classifier is to collect enough cases for each of the categories. The other 10 subtypes of RCCs and emerging/provisional entities not included in this model, together represent less than 5% of RCCs. AI-based systems' performance tends to correlate with the size of the datasets. There is a limited number of open datasets with WSIs of RCC subtypes and other types of renal neoplasms. The Cancer Genome Atlas (TCGA) repository has datasets with WSIs of ccRCC, pRCC, and chRCC that were used by other investigators.[12,13,21] But there are no large-scale datasets able to provide enough cases of rare subtypes of tumor to investigate more comprehensive computational approaches. To address the lack of data, multi-institutional collaborations with focus on AI for pathology are emerging. The BIGPICTURE project initiated in Europe aims to create large-scale datasets of WSIs from academics, small enterprises, and pharmaceutical companies to unlock the next generation of AI research in pathology. In the US, the National Institutes of Health recently provided funding opportunities for projects to generate data for AI research.[26]

Several limitations need to be considered. The WSI validation dataset only included slides of nephrectomy specimens. Further investigation is needed to determine the classification performance on biopsy specimens. The increased incidence of pRCC cases is a result of data re-utilization from a previous project. This methodology presents the advantage of enlarging the dataset and undergoing evaluation and validation by multiple pathologists. Despite this, it may also introduce a selection bias. However, as the cases were processed within the same laboratory, the impact of the bias may be unsubstantial.

Grading is a critical aspect in the evaluation of RCC. A random sample of ccRCC cases was obtained and, as anticipated, most of the tumors analyzed were grades 2 and 3. An analysis of grade subgroup performance was not conducted due to the intricacy of the task. The presence of grade heterogeneity within a single WSI is a common occurrence in RCC. The final grade is determined based on the area with the highest grade; pixel-level annotation was not available in our dataset to conduct detailed analysis. We acknowledge that the model's performance may be impacted by an increase in the number of high-grade tumors. One example of a misclassified ccRCC case had dominant rhabdoid features, which was not a morphology adequately represented in the training set.

The aggregate analysis of patches of the WSI dataset by majority vote is a naïve technique to create a final diagnostic label, but nevertheless, it showed promising results and is easy to interpret. Recurrent neural networks are an example of AI-based technique that can be used to optimize the results of patch aggregation.[27]

In conclusion, we demonstrated the performance of an AI-based model that showed potential for accuracy for automatic diagnosis of 6 subtypes of neoplasms on WSI. However, large scale multi-institutional validations studies are needed to verify the reproducibility of the system.

Author contributions

All authors have made substantial contributions to conception and design, or acquisition of data, or analysis and interpretation of data.

All authors have been involved in drafting the manuscript or revising it critically for important intellectual content.

All authors have given final approval of the version of this manuscript for publication.

Disclosures/Conflict of interest

The authors have nothing to disclose.

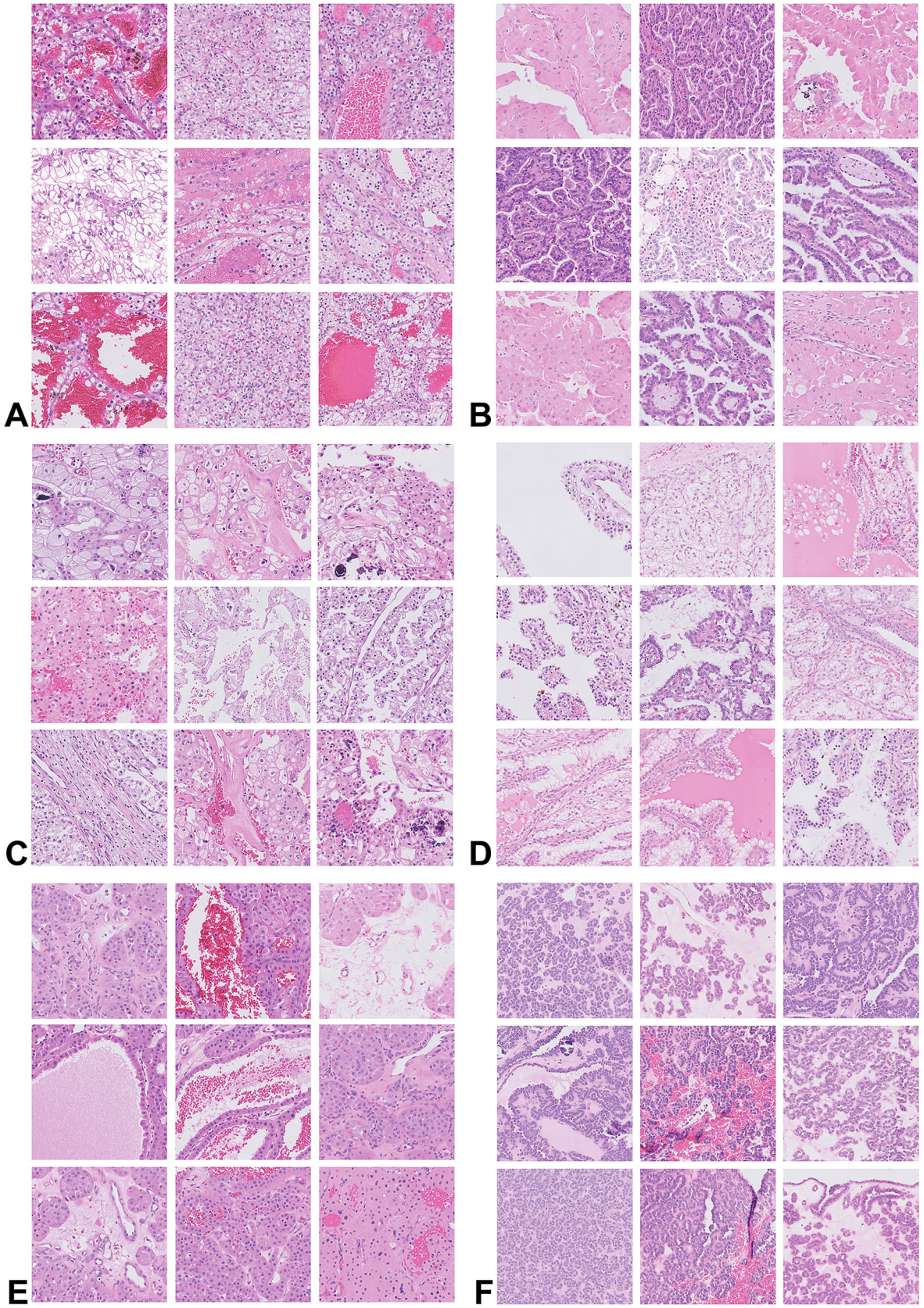

Fig. 5. Patches in agreement with original diagnosis showing more than 90% likelihood of belonging to these categories: (A) clear cell renal cell carcinoma; (B) papillary renal cell carcinoma; (C) chromophobe renal cell carcinoma; (D) clear cell papillary cell carcinoma; (E) oncocytoma; and (F) metanephric adenoma.

Acknowledgments

The authors acknowledge the Indiana University Pervasive Technology Institute for providing HPC (Big Red II and Karst) and access to UITS Advanced Visualization Lab; resources that have contributed to the research results reported. https://pti.iu.edu/.

Natasha Gibson for digitalization of glass slides at Indiana University.

We would like to thank the late Dr. David Grignon (Indiana University) for reviewing a subset of cases and sharing his expert opinion.

Appendix A. Supplementary data

Supplementary data to this article can be found online at https://doi.org/10.1016/j.jpi.2023.100299.

References

1. Padala SA, Barsouk A, Thandra KC, Saginala K, Mohammed A, Vakiti A, et al. Epidemiology of renal cell carcinoma. World J Oncol 2020;11:79–87.
2. Vasudev NS, Wilson M, Stewart GD, Adeyoju A, Cartledge J, Kimuli M, et al. Challenges of early renal cancer detection: symptom patterns and incidental diagnosis rate in a multicentre prospective UK cohort of patients presenting with suspected renal cancer. BMJ Open 2020;10, e035938.
3. Zhou H, Zheng S, Truong LD, Ro JY, Ayala AG, Shen SS. Clear cell papillary renal cell carcinoma is the fourth most common histologic type of renal cell carcinoma in 290 consecutive nephrectomies for renal cell carcinoma. Hum Pathol 2014;45:59–64.
4. Colling R, Pitman H, Oien K, Rajpoot N, Macklin P, Snead D, et al. Artificial intelligence in digital pathology: a roadmap to routine use in clinical practice. J Pathol 2019;249:143–150.
5. Ström P, Kartasalo K, Olsson H, Solorzano L, Delahunt B, Berney DM, et al. Pathologist-level grading of prostate biopsies with artificial intelligence. ArXiv 2019. abs/1907.01368: https://arxiv.org/abs/1907.01368.
6. Abels E, Pantanowitz L, Aeffner F, Zarella MD, van der Laak J, Bui MM, et al. Computational pathology definitions, best practices, and recommendations for regulatory guidance: a white paper from the digital pathology association. J Pathol 2019;249:286–294.
7. LeCun Y, Bengio Y, Hinton G. Deep learning. Nature 2015;521:436–444.
8. Goodfellow I, Bengio Y, Courville A. *Deep Learning*. Cumberland: MIT Press. 2016.
9. Rawat W, Wang Z. Deep convolutional neural networks for image classification: a comprehensive review. Neural Comput 2017;29:2352–2449.
10. Sultana F, Sufian A, Dutta P. Advancements in image classification using convolutional neural network. 2018 Fourth International Conference on Research in Computational Intelligence and Communication Networks (ICRCICN). Kolkata, India; 2018. p. 122–129.
11. Hinton G. Deep learning-A technology with the potential to transform health care. JAMA 2018;320:1101–1102.
12. Tabibu S, Vinod PK, Jawahar CV. Pan-renal cell carcinoma classification and survival prediction from histopathology images using deep learning. Sci Rep 2019;9:10509.
13. Fenstermaker M, Tomlins SA, Singh K, Wiens J, Morgan TM. Development and validation of a deep-learning model to assist with renal cell carcinoma histopathologic interpretation. Urology 2020;144:152–157.
14. Gayhart M, Prater A, Smith S. "Virtual" biomarkers? Convolutional neural networks can accurately distinguish chromophobe from clear cell renal cell carcinoma. Abstract 1548 from USCAP 2020: Informatics. Lab Invest, 100; 2020. p. 1456.
15. Cheng J, Han Z, Mehra R, Shao W, Cheng M, Feng Q, et al. Computational analysis of pathological images enables a better diagnosis of TFE3 Xp11.2 translocation renal cell carcinoma. Nat Commun 2020;11:1778.
16. Google. Google Cloud AutoML. https://cloud.google.com/automl 2019.
17. Google. AutoML Vision Beginner's guide. https://cloud.google.com/vision/automl/docs/beginners-guide 2019.
18. CodePlex Foundation. OpenSeadragon: An Open-Source, Web-Based Viewer for High-Resolution Zoomable Images, Implemented in Pure JavaScript, for Desktop and Mobile. http://openseadragon.github.io 2009.
19. Web Technology for Developers–CSS: Cascading Style Sheets. https://developer.mozilla.org/en-US/docs/Web/CSS 2021.
20. FDA News Release: FDA Authorizes Software that can Help Identify Prostate Cancer. https://www.fda.gov/news-events/press-announcements/fda-authorizes-software-can-help-identify-prostate-cancer 2021.
21. Laleh NG, Muti HS, Lavinia Loeffler CM, Echle A, Saldanha OL, Mahmood F, et al. Benchmarking artificial intelligence methods for end-to-end computational pathology. bioRxiv 2021.2021.08.09.455633: https://www.biorxiv.org/content/10.1101/2021.08.09.455633v1.
22. Abdeltawab H, Khalifa F, Ghazal M, Cheng L, Gondim D, El-Baz A. Author Correction: a pyramidal deep learning pipeline for kidney whole-slide histology images classification. Sci Rep 2021;11:21867.
23. Abdeltawab H, Khalifa F, Ghazal M, Cheng L, Gondim D, El-Baz A. A pyramidal deep learning pipeline for kidney whole-slide histology images classification. Sci Rep 2021;11:20189.
24. Trpkov K, Yilmaz A, Uzer D, Dishongh KM, Quick CM, Bismar TA, et al. Renal oncocytoma revisited: a clinicopathological study of 109 cases with emphasis on problematic diagnostic features. Histopathology 2010;57:893–906.
25. Moch H, Humphrey PA, Ulbright TM, Reuter VE. *International Agency for Research on Cancer. WHO Classification of Tumours of the Urinary System and Male Genital Organs.* Lyon: International Agency for Research on Cancer. 2016.
26. National Institutes of Health. Bridge to Artificial Intelligence (Bridge2AI). https://commonfund.nih.gov/bridge2ai 2021.
27. Kanavati F, Toyokawa G, Momosaki S, Takeoka H, Okamoto M, Yamazaki K, et al. A deep learning model for the classification of indeterminate lung carcinoma in biopsy whole slide images. Sci Rep 2021;11:8110.